Proceedings of the Combustion Institute, Volume 28, 2000/pp. 1349–1357

CATALYTIC COMBUSTION OF METHANE/AIR MIXTURES OVER PLATINUM: HOMOGENEOUS IGNITION DISTANCES IN CHANNEL FLOW CONFIGURATIONS

JOHN MANTZARAS, CHRISTOPH APPEL AND PETER BENZ
Paul Scherrer Institute
Combustion Research
CH-5232 Villigen-PSI, Switzerland

The homogeneous ignition of fuel-lean methane/air mixtures is investigated numerically in laminar plane channel configurations with platinum-coated isothermal walls and uniform incoming properties. Parametric studies are carried out to determine the dependence of the homogeneous ignition distance (x_{ig}) on the fuel-to-air equivalence ratio (ϕ), the wall temperature (T_W), the inlet temperature (T_{IN}), the inlet velocity (U_{IN}), and the channel wall separation ($2b$). Computations are performed with elliptic and parabolic two-dimensional numerical codes, both with elementary heterogeneous and homogeneous chemical reaction schemes. The applicability of the parabolic approach (boundary layer approximation) in assessing homogeneous ignition is investigated. The elliptic approach yields shorter x_{ig} compared to those of the parabolic approach, but as U_{IN} increases, their difference diminishes, and for U_{IN} greater than a minimum value $U_{m,IN}$, both computations give the same x_{ig}. $U_{m,IN}$ depends strongly on ϕ and ranges from 8 m/s (ϕ = 0.35) to 15.5 m/s (ϕ = 0.55) at atmospheric pressure. An analytical homogeneous ignition criterion based on activation energy asymptotics, a one-step gaseous reaction and a mass-transport-limited surface reaction, is presented for catalytic channel configurations and adapted to lean methane/air combustion. The mass-transport-limited assumption is shown to be valid only at atmospheric pressure. A one-step gaseous reaction with a methane order of -0.33 and an activation energy of 243.4 kJ/mol yields, in conjunction with the analytical ignition criterion, homogeneous ignition distances at atmospheric pressure within 9.2% of those numerically predicted over a wide range of operating conditions ($0.35 \leq \phi \leq 0.55$, 1380 K $\leq T_W \leq$ 1600 K, 623 K $\leq T_{IN} \leq$ 743 K and 1.5 mm $\leq b \leq$ 15 mm). The negative methane reaction order (methane self-inhibition) results in shorter x_{ig} for the leaner mixtures. The apparent activation energy is higher than that of purely homogeneous combustion (~200 kJ/mol) due to catalytic inhibition via radical adsorption.

Introduction

Catalytically stabilized combustion (CSC) is investigated for potential application to gas-fired turbines. The current efforts are directed toward the hybrid approach whereby nearly half of the fuel is burned heterogeneously in staged catalytic modules and the rest is combusted in a postcatalyst gaseous reactor [1]. The temperatures reached at the gaseous reactor outlet are those required by current generation turbines (1450 to 1775 K). The onset of homogeneous ignition within the catalytic modules is detrimental to the catalyst integrity, and this problem is further accentuated by the current trend to use higher-temperature catalysts. The coupling of heterogeneous/homogeneous chemical reactions leading to homogeneous ignition is hence one important aspect in CSC research.

The homogeneous ignition in catalytic combustion has been investigated primarily in one-dimensional stagnation point flows [2–4]. Extending previous studies, we investigated numerically [5] the homogeneous ignition of methane/air mixtures in channel CSC using a two-dimensional elliptic model with elementary gaseous and surface reactions. Predictions with this model were successfully compared to measurements at atmospheric pressure [6], strengthening the confidence on the CSC applicability of newly developed surface reaction schemes [7]. Recently [8], we investigated homogeneous ignition in laminar channel CSC using matched activation energy asymptotics and simplified chemistry; an analytical ignition criterion was obtained for the homogeneous ignition distance in terms of the relevant geometrical, flow, transport, and chemical parameters. In the present study, we undertake a detailed numerical investigation of homogeneous ignition of lean methane/air mixtures in channels with platinum-coated isothermal walls and uniform incoming properties. Parametric studies are carried out by varying the channel hydraulic diameter, the fuel-to-air equivalence ratio, the wall temperature, the preheat temperature, and the incoming velocity. The main objective is to provide an analytical ignition criterion, based on the established functional form [8], that

can predict with good accuracy homogeneous ignition distances in methane/air CSC. A particular objective is to assess the adequacy of the boundary layer approximation in determining homogeneous ignition.

Method of Approach

The plane channel consists of two catalytically active parallel walls placed at a distance $2b$ apart. Both walls have temperature T_W, and the incoming flow has uniform properties (temperature T_{IN}, velocity U_{IN}, and species mass fractions $Y_{i,IN}$).

Analytical Approach

The key elements of the analytical approach are presented next (details are given in Ref. [8]). The approach is based on matched activation energy asymptotics in conjuntion with the boundary layer approximation, a one-step gaseous reaction ($F + \nu_O O \rightarrow \nu_P P$), and an infinitely fast catalytic reaction. The Prandtl (Pr) number, Lewis (Le) number, and c_p are constant. For a gaseous reaction rate (see nomenclature section),

$$\omega_F = W_F B T^{\gamma} \left(\frac{\rho Y_F}{W_F}\right)^{n_F} \left(\frac{\rho Y_O}{W_O}\right)^{n_O} \exp(-E/RT) \tag{1}$$

the closed-form ignition criterion is

$$\zeta_{ig} \frac{F(\zeta_{ig})}{\Delta^*_{cr}(\zeta_{ig})} = \frac{1}{2Pr} A \frac{1}{Da} \tag{2}$$

with ζ_{ig} the non-dimensional ignition distance

$$\zeta_{ig} = x_{ig}/(bRePr) \text{ and } Re = \rho_{IN} U_{IN} b/\mu_{IN} \tag{3}$$

The Damköhler number (Da) is the ratio of a characteristic transverse diffusion time to a characteristic gaseous chemical time, $Da = \tau_d/\tau_{ch}$, with

$$\tau_d = \frac{b^2}{\alpha_{th,IN}},\ \tau_{ch} = \left[B\left(\frac{p\bar{W}}{R}\right)^{n-1} \left(\frac{W_F^{1-n_F}}{W_O^{n_O}}\right) T_W^{1+\gamma-n} \left(Y_{O,IN} - \frac{W_O \nu_O}{W_F} Y_{F,IN}\right)^{n_O} Y_{F,IN}^{n_F} \exp\left(-\frac{E}{RT_W}\right)\right]^{-1} \tag{4}$$

The parameter A and the function $F(\zeta)$ in equation 2 are

$$A = \frac{(T_W - T_{IN})^{2+n_F}}{T_W^{2(1+n_F)} \left(\frac{R}{E}\right)^{1+n_F} \left(\frac{q}{c_p}\right)},\ F(\zeta) = \frac{Le^{n_F(1/3+0.19\zeta^{0.35})}}{\left[(0.43 + 0.45\zeta^{0.35}) Pr^{1/3+0.242\zeta^{0.2}} \left(\frac{T_W}{T_{IN}}\right)^{0.774\zeta^{0.2}}\right]^2} \tag{5}$$

Finally, Δ^*_{cr} in equation 2 is the critical ignition Damköhler number defined as the value of Δ_{cr} for which equation 6 gives a unique solution for the temperature perturbation gradient $(\partial\varphi/\partial\chi)_{\chi=0}$ corresponding to thermal runaway:

$$\frac{d^2\varphi}{d\chi^2} = -\Delta_{cr} (\chi - \alpha\varphi)^{n_F} \exp(\varphi - \chi)$$

$$\text{subject to } \varphi(0) = 0 \text{ and } (\partial\varphi/\partial\chi)_{\chi\rightarrow\infty} = 0 \tag{6}$$

with

$$\alpha = \frac{Le^{2/3-0.19\zeta^{0.35}} (T_W - T_{IN}) c_p}{Y_{F,IN} q} \tag{7}$$

Δ^*_{cr} is a function of ζ (albeit weak) due to the ζ dependence of α. Equation 2 is valid over the parameter range

$$0.002 \le \zeta \le 0.16,\ 1.5 \le T_W/T_{IN} \le 3.0,$$
$$\text{and } 0.9 \le Le \le 2.0 \tag{8}$$

The temperature and Lewis number ranges are of particular interest to hydrocarbon CSC. The left-hand side of equation 2 is a monotonically increasing function of ζ (see Ref. [8]), resulting in an increase of ζ_{ig} with decreasing Da. The chemical and transverse diffusion time scales appearing in Da demonstrate the competition between surface and gaseous reactions. Short diffusion times (small channel half-widths b) favor catalytic depletion and therefore inhibit gaseous ignition, while short chemical times (or large b) favor gaseous ignition.

Numerical Approach

Computations were performed with elliptic and parabolic two-dimensional codes, both with elementary surface and gaseous reaction schemes. The elliptic code (Navier–Stokes equations) is a finite-volume approach and has been described in detail elsewhere [5,6]. In the parabolic approach (boundary layer approximation), the computer program DASSL [9] was employed. DASSL was used with detailed surface chemistry in purely heterogeneous combustion [10] and with one-step gaseous reaction in our earlier work [8]. For lean combustion, the C_1/H/O gaseous mechanism by Warnatz [11] was employed (108 reactions and 17 species). For surface chemistry, the Pt scheme by Deutschmann et al. [7] was used (26 reactions, 7 gaseous species, and 11 surface species). The surface site density was 2.7×10^{-9} mol/cm^2, simulating polycrystalline platinum [6,7].

The inlet temperature ranged between 623 and 743 K (typical combustor inlet temperatures in gas turbines), and the fuel-to-air equivalence ratio (ϕ) ranged between 0.35 and 0.55, resulting in adiabatic flame temperatures (T_{af}) of 1428 to 1930 K, a range encompassing the inlet temperatures of gas turbines.

The highest wall temperature T_W was 1600 K, an upper limit already high for catalyst stability. The lowest T_W was determined by the requirement of ignition at the longest distance of equation 8 (ζ = 0.16) with b not exceeding 10 mm. The independent control of T_W and ϕ is of practical interest as T_W can be lower than T_{af} due to finite-rate surface kinetics and non-adiabatic operation. The employed isothermal wall boundary condition has wider application than the adiabatic wall boundary condition; under the mass-transport-limited assumption of equation 2, and for a diffusionally balanced fuel with $Le = 1$ (methane has $Le \approx 0.95$), the latter boundary condition yields T_W equal to T_{af}. In the approach of this study, the wall temperature is allowed to be lower (or higher) than T_{af}.

In the elliptic approach, successive grid refinement led to a grid-independent solution; up to 20,000 control-volumes were used. In the parabolic approach, up to 400 transverse grid points were used; forward integration (marching in x) provided the solution up to the desired x distance. The CPU time was ~28 h for the elliptic and ~15 min for the parabolic code in an α-cluster machine.

Results and Discussion

Comparison Between Elliptic and Parabolic Predictions

The adequacy of the boundary layer approximation in assessing homogeneous ignition is investigated. Computed elliptic (a1 to j1) and parabolic (a2 to j2) OH distributions are presented in Fig. 1. The ignition locations indicated by arrows were determined from Fig. 2. The local catalytic fuel conversion C, the integrated (over b) gaseous fuel conversion G, and the average (over b) OH mass fraction Y_{OH} are plotted in Fig. 2 for flame a2 of Fig. 1. The sharp rise in either G or Y_{OH} yields essentially the same ignition distance; the rise in Y_{OH} is used henceforth to define x_{ig}. In Fig. 1a–c, only ϕ was varied. The leaner mixtures ignite earlier in both elliptic and parabolic computations. The self-inhibiting role of methane is already established [12,13] for purely homogeneous combustion. The presence of a catalytic surface does not alter the self-inhibition. The elliptic computations (Fig. 1a1–c1) yield shorter x_{ig} compared to their parabolic counterparts (Fig. 1a2–c2), but as ϕ decreases their discrepancy diminishes. The key parameters determining the agreement between both types of computations are ϕ and U_{IN}. The flame stabilization in CSC involves the near-wall homogeneous/heterogeneous chemical interactions and the flame propagation inside the boundary layer. The average flame sweep angle (acute angle of the flamefront with respect to the x axis) increases with increasing ϕ due to the corresponding increase in the local laminar flame speed. Therefore, the richer mixtures have a larger axial flame component, leading to a considerable contribution of upstream propagation in the flame stabilization process. The last aspect is suppressed in the parabolic approach (no axial diffusion).

The effect of inlet velocity is discussed separately in Fig. 1d and e, with U_{IN} = 5 and 12 m/s, respectively, and b = 2 mm, ϕ = 0.50, T_W = 1600 K, and T_{IN} = 623 K. The parabolic predictions in Fig. 1d2 and e2 yield exactly the same ζ_{ig}, while x_{ig} are linearly proportional to U_{IN}. The former is evident from equation 2 (independent of U_{IN}), and the latter from equation 3 (for a fixed ζ_{ig}, x_{ig} are proportional to U_{IN}). The increase in U_{IN} reduces the flame sweep angle (note the x-scale change in Fig. 1d and e) and hence improves the agreement between parabolic and elliptic predictions. At U_{IN} = 12 m/s, both computations in Fig. 1e yield essentially the same x_{ig}. The minimum U_{IN} required to reach the parabolic limit is further denoted as $U_{m,IN}$. Although for all $U_{IN} \geq U_{m,IN}$ the parabolic limit is obtained, the present laminar formulation holds for $Re \leq 1000$ (Re is based on b).

The influence of T_{IN}, T_W and b on $U_{m,lN}$ is weaker. In Fig. 1f, T_{IN} is increased to 743 K (the other parameters are as in Fig. 1e). The elliptic ζ_{ig} is ~3% lower than its parabolic counterpart, indicating an increase of $U_{m,IN}$ with increasing T_{IN}. In Fig. 1g, the halfwidth is increased to b = 6 mm (the other parameters are as in Fig. 1e). Increasing b results in shorter ζ_{ig} which, in turn, leads to a flame with higher effective gaseous fuel concentration (the catalytic fuel conversion increases with ζ, as will be discussed in Fig. 5) but with reduced bulk gaseous preheat due to reduced contact with the hot wall; both effects do not balance exactly, since the system is non-adiabatic leading to an elliptic ζ_{ig} that is ~5% shorter than the parabolic one and, hence, to somewhat increased requirements for $U_{m,IN}$. Finally, $U_{m,IN}$ decreases with reduction of T_W; in Fig. 1h (T_W = 1450 K, b = 10 mm), $U_{m,IN}$ is shown to be 11.5 m/s. For atmospheric pressure combustion, $U_{m,IN}$ were calculated under the most stringent conditions (T_W = 1600 K, T_{IN} = 743 K). For ϕ = 0.35, 0.40, 0.45, 0.50, and 0.55, the computed $U_{m,IN}$ were 8.0, 11.0, 13.0, 14.5, and 15.5 m/s, respectively. Atmospheric CSC test rigs have usually high U_{IN}, but they do not always meet the $U_{m,IN}$ requirements (20 m/s $\leq U_{IN}$ [14], 10 m/s $\leq U_{IN}$ [15]). The determination of $U_{m,IN}$ is of prime interest in CSC modeling due to the substantially lower parabolic CPU requirements. It is emphasized that the controlling parameter in the above comparisons is the absolute magnitude of U_{IN} and not geometrical factors (b) or non-dimensional groups (such as Re) with an explicit geometric dependence.

At higher pressures, the reduction in the laminar flame speed resulted in lower $U_{m,IN}$. In Fig. 1i (p = 2 bar) and 1j (p = 4 bar), velocities of 5.5 m/s and

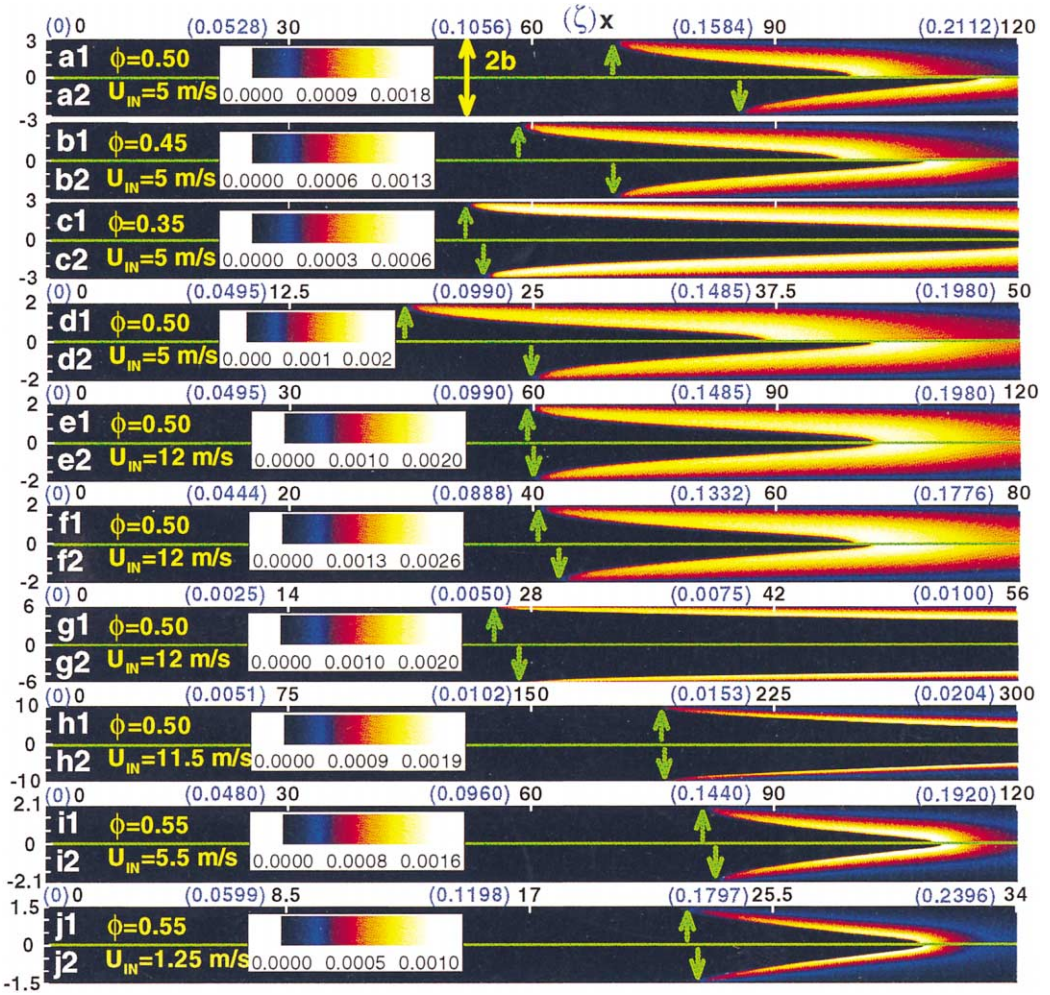

FIG. 1. Two-dimensional maps of the OH mass fraction. For each flame (a to j), the upper half of the channel (a1 to j1) corresponds to elliptic predictions and the lower half (a2 to j2) to parabolic predictions. Streamwise distances are given in physical (x) and nondimensional (ζ) coordinates; the ζ distances are indicated with blue color. All physical distances are in millimeters. The green arrows indicate the location of homogeneous ignition. The color bar in each figure part indicates the OH mass fraction levels. (a) $\phi = 0.50$, $U_{IN} = 5$ m/s, $T_W = 1500$ K, $T_{IN} = 623$ K, $b = 3$ mm, and $p = 1$ bar. (b) $\phi = 0.45$, $U_{IN} = 5$ m/s, $T_W = 1500$ K, $T_{IN} = 623$ K, $b = 3$ mm, and $p = 1$ bar. (c) $\phi = 0.35$, $U_{IN} = 5$ m/s, $T_W = 1500$ K, $T_{IN} = 623$ K, $b = 3$ mm, and $p = 1$ bar. In (a), (b), and (c) the x and ζ distances are the same; the change in Re and Pr (due to variation in ϕ) results in a small ($\sim$1%) change in ζ which is, however, not shown. (d) $\phi = 0.50$, $U_{IN} = 5$ m/s, $T_W = 1600$ K, $T_{IN} = 623$ K, $b = 2$ mm, and $p = 1$ bar. (e) $\phi = 0.50$, $U_{IN} = 12$ m/s, $T_W = 1600$ K, $T_{IN} = 623$ K, $b = 2$ mm, and $p = 1$ bar. (f) $\phi = 0.50$, $U_{IN} = 12$ m/s, $T_W = 1600$ K, $T_{IN} = 743$ K, $b = 2$ mm, and $p = 1$ bar. (g) $\phi = 0.50$, $U_{IN} = 12$ m/s, $T_W = 1600$ K, $T_{IN} = 623$ K, $b = 6$ mm, and $p = 1$ bar. (h) $\phi = 0.50$, $U_{IN} = 11.5$ m/s, $T_W = 1450$ K, $T_{IN} = 623$ K, $b = 10$ mm, and $p = 1$ bar. (i) $\phi = 0.55$, $U_{IN} = 5.5$ m/s, $T_W = 1500$ K, $T_{IN} = 623$ K, $b = 2.1213$ mm, and $p = 2$ bar. (j) $\phi = 0.55$ $U_{IN} = 1.25$ m/s, $T_W = 1500$ K, $T_{IN} = 623$ K, $b = 1.5$ mm, and $p = 4$ bar. The b values in flames (i) and (j) are such that the diffusion times τ_d are equal ($\alpha_{th,IN} \propto 1/p$).

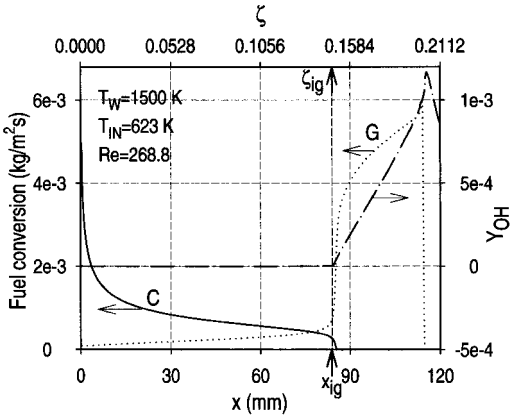

FIG. 2. Streamwise profiles of local catalytic (C, solid line) and gaseous (G, dotted line) fuel conversion rates for the flame a2 of Fig. 1. The catalytic conversion refers to one wall, and the volumetric gaseous rate has been integrated over the channel halfwidth b. The average (over b) OH mass fraction (Y_{OH}, dashed-dotted line) is also given. The onset of homogeneous ignition is defined by the sharp rise in the OH profile. Both in physical (x) and non-dimensional (ζ) streamwise distances are given.

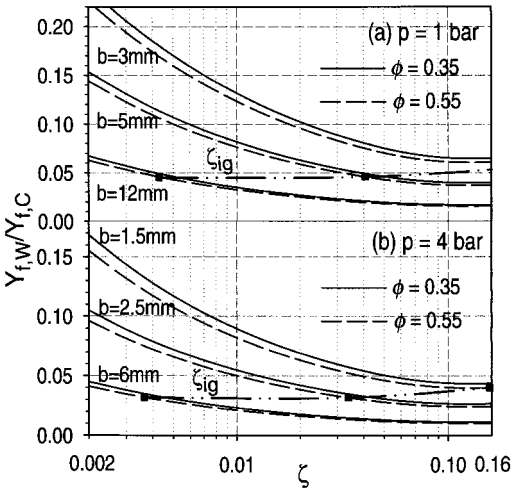

FIG. 3. Streamwise profiles of the ratio of wall ($Y_{f,W}$) to channel-center ($Y_{f,C}$) methane mass fractions for T_W = 1500 K, T_{IN} = 623 K, two equivalence ratios (solid lines ϕ = 0.35 and dashed lines ϕ = 0.55), three b values, and two pressures: (a) p = 1 bar and (b) p = 4 bar. The computations of Fig. 3 pertain to purely heterogeneous combustion. The solid symbols are the corresponding ignition distances ζ_{ig} (calculated with both surface and gaseous schemes) for ϕ = 0.55. In Fig. 3a, for b = 3 mm $\zeta_{ig} >$ 0.16.

1.25 m/s, respectively, were sufficient for good agreement between both computations. $U_{m,IN}$ at high pressures are not reported since, as discussed next, the ignition criterion is applicable at atmospheric pressure.

Finite-Rate Surface Kinetics

Equation 2 was derived for mass-transport-limited surface reactions. To assess the importance of finite-rate surface kinetics, computations were performed with the gaseous chemistry turned off. The ratio of the wall-to-center methane mass fraction $Y_{f,W}/Y_{f,C}$ is plotted in Fig. 3 ($Y_{f,W}/Y_{f,C}$ is identically zero under mass-transport-limited conditions). Finite-rate surface kinetics are more pronounced at shorter ζ, smaller b, lower pressures, and lower ϕ. The purely heterogeneous computations of Fig. 3 were virtually independent of U_{IN} and model type, while the influence of ϕ was weak. The lowest and highest b in Fig. 3 are representative values for ignition at the low (ζ = 0.002) and high ($\zeta \approx 0.16$) ends, respectively. The loci of ζ_{ig} (parabolic predictions) is also shown in Fig. 3 for ϕ = 0.55; at ignition, $Y_{f,W}/Y_{f,c}$ is always less than 6.5% at p = 1 bar and less than 4.5% at p = 4. To assess whether such levels are sufficiently low for the mass-transport-limited formulation of equation 2, ignition was studied with full gaseous and surface reactions but with the heterogeneous rates artificially increased by a factor K ranging from 2 to 40. The adsorption/desorption radical reactions were kept at their normal values (K = 1) to eliminate promotion/inhibition on gaseous ignition. The last step, however, proved unnecessary since the simultaneous increase by a factor of up to 40 of the adsorption and desorption of the cardinal OH radical [5] did not produce noticeable changes in ζ_{ig}. The calculated ζ_{ig}, further denoted as $\zeta_{ig}(K)$, increase with increasing K for K up to 10 and then remain essentially constant. Moreover, $\zeta_{ig}(K = 10)$ are only moderately larger than $\zeta_{ig}(K = 1)$. In Fig. 3a and for b = 3 mm, for example, $\zeta_{ig}(K = 10)$ is 7.2% higher than $\zeta_{ig}(K = 1)$. In all atmospheric-pressure applications, $\zeta_{ig}(K = 10)$ is 1%–12% higher than $\zeta_{ig}(K = 1)$. At higher pressures, however, the corresponding increase is significantly larger (up to 28% at p = 2 bar and up to 40% at p = 4 bar). This happens despite the fact that $Y_{f,W}/Y_{f,C}$ is smaller at high pressures. The reason is illustrated in Fig. 4, in which computed transverse profiles (with normal surface rates) of Y_{CH_4}, Y_{OH}, and the methane gaseous reaction rate are presented at $\zeta_i = \zeta_{ig}$ for three pressures. As pressure increases, the gaseous combustion moves closer to the wall in regions of substantially lower fuel levels; such low levels are sensitive to the particular surface reaction rates. Finite-rate surface kinetics must be thus included explicitly in a high-pressure ignition formulation. Therefore, the ignition criterion of equation 2 will

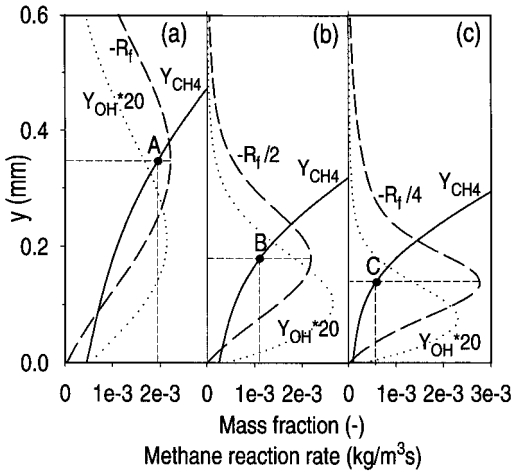

FIG. 4. Transverse (y) profiles of the methane mass fraction (solid lines), the OH mass fraction (dotted lines), and the methane gaseous reaction rate (R_f, dashed lines) at ignition ($\zeta = \zeta_{ig}$): (a) $p = 1$ bar, (b) $p = 2$ bar, and (c) $p = 4$ bar. The other parameters are $\phi = 0.50$, $T_W = 1500$ K, $T_{IN} = 623$, $U_{IN} = 5$ m/s, and $b = 3$ mm. The wall is located at $y = 0$, and only the region extending 0.6 mm away from the wall is shown. The points A, B, and C indicate the methane mass fractions at the location of maximum methane reaction rate R_f. With increasing pressure, the transverse location of the maximum reaction rate approaches the wall.

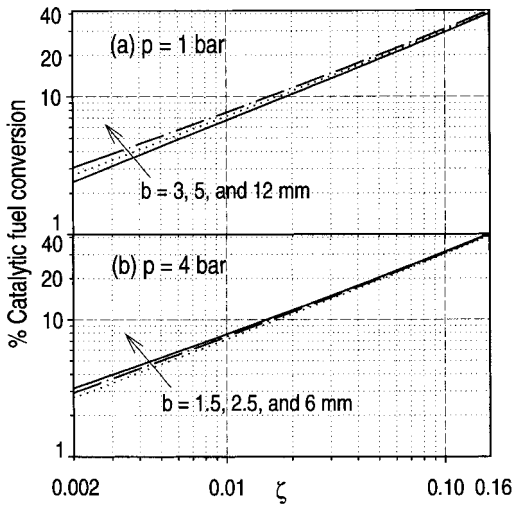

FIG. 5. Percentage of methane catalytic conversion for three halfwidths b and two pressures: (a) $p = 1$ bar and (b) $p = 4$ bar. The arrows indicate the direction of increasing b. Purely heterogeneous computations for $T_W = 1500$ K and $T_{IN} = 623$ K.

be examined at $p = 1$ bar. In any case, experimental verification on homogeneous ignition with the present reaction schemes exists only at $p = 1$ bar [6].

The streamwise range $0.002 \leq \zeta_{ig} \leq 0.16$ is sufficient for CST. This is illustrated in the catalytic fuel-conversion plots of Fig. 5 (computed with the gaseous chemistry turned off). The catalytic conversion is virtually independent of U_{IN} and ϕ and mildly dependent on b; the conversion at $\zeta = 0.16$ is in the range of 39.6%–41.9% ($p = 1$ bar) and 40.6%–42% ($p = 4$ bar). When $T_W = 1600$ K and $p = 1$ bar, the conversion ranges from 38.4%–42.1%. Since hybrid CST designs employ a sequence of two modules with a combined ~50% conversion [1], it is unlikely that each module exceeds the above-determined ~40% conversion.

Ignition Distances

Extensive parabolic computations were performed at atmospheric pressure. Five ϕ (0.35, 0.40, 0.45, 0.50, and 0.55), three T_{IN} (623, 683, and 743 K) and six T_W (1600, 1550, 1500, 1450, 1400, and 1380 K) were examined. The lowest T_W was 1380 K, set by the requirement of $\zeta_{ig} = 0.16$ with b not exceeding 10 mm (for all ϕ and T_{IN}); at $T_W = 1350$ K, for example, $\zeta_{ig} = 0.16$ for $b \geq 11$ mm. The particular U_{IN} is not relevant in the parabolic approach; $U_{IN} = 15$ m/s was chosen for all computations. For every set of computations (fixed ϕ, T_{IN}, and T_W) up to fourteen b were used. The minimum, b_{min}, yielded $\zeta_{ig} = 0.16$. The maximum, b_{max}, gave $\zeta_{ig} = 0.002$ as long as $b_{max} \leq 15$ mm, otherwise the shortest ζ_{ig} was calculated for $b_{max} = 15$ mm; channels with $b_{max} > 15$ mm are, in any case, of little interest to confined configurations.

The full parabolic computations were compared to analytical predictions with a one-step reaction $CH_4 + 2O_2 \rightarrow CO_2 + 2H_2O$. The parameters in equation 2 were $Le = 0.95$, $Pr = 0.706$, $q = 50028$ kJ/kg, $W_F = 16$ kg/kmol, $W_O = 32$ kg/kmol, $\bar{W} = 28.2$ kg/kmol, and $\nu_O = 2$. The c_p at a given ϕ was the average between T_{IN} and T_W; c_p ranged from 1.196 kJ/kgK to 1.267 kJ/kgK. The gaseous kinetic parameters (equation 1) were determined as follows. For atmospheric-pressure combustion, the oxidizer order n_O was set to zero (for fuel-lean combustion, n_O is of main use to give the correct pressure dependence via the total reaction order n). The fuel reaction order n_F was determined by fitting equation 2 to computed ζ_{ig} at different ϕ and fixed T_W, T_{IN}, and b. An iterative process was established since n_F is included in Δ^*_{cr} and Da. A value of n_F was initially guessed, equation 6 was solved to provide Δ^*_{cr}, and finally an updated value of n_F was sought in Da so that equation 2 gave the best fit to the numerically predicted ζ_{ig}. The iterative process is illustrated in the insert of Fig. 6, with a converged value of $n_F =$

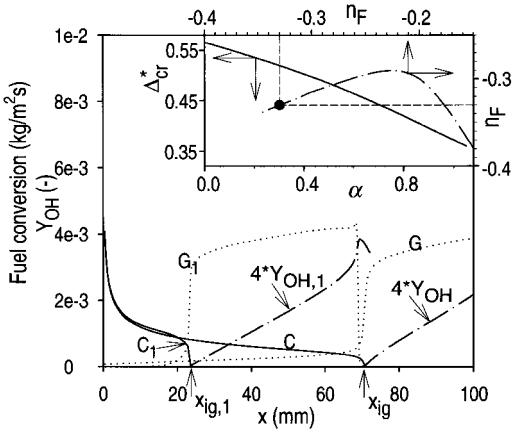

FIG. 6. Streamwise profiles of local catalytic fuel conversion (C and C_1, solid lines), gaseous fuel conversion (G and G_1, dotted lines) and OH mass fraction (Y_{OH} and $Y_{OH,1}$, dashed-dotted lines) for $\phi = 0.45$, $T_W = 1500$ K, $T_{IN} = 623$ K (parabolic computations). Two cases are presented: full surface reaction scheme (C, G, Y_{OH}) and surface scheme with adsorption/desorption of OH and adsorption of O and H removed (C_1, G_1, $Y_{OH,1}$). In the inset, the iterative procedure for calculating the fuel reaction order is illustrated. The horizontal axis is the initial guess of n_F, and the vertical axis the updated one; convergence is at $n_F = -0.33$. In the inset, the plot of Δ^*_{cr} versus α is shown (for $n_F = -0.33$). A polynomial fit is also provided for Δ^*_{cr}:

$$\Delta^*_{cr}(\alpha) = \sum_{k=1}^{6} A_k \alpha^{k-1}$$

$A_1 = 0.5664$, $A_2 = -0.1465$, $A_3 = -4.638 \times 10^{-4}$, $A_4 = -0.0701$, $A_5 = -0.0105$, and $A_6 = 0.0332$.

-0.33. The calculated n_F is consistent with literature values ($n_F = -0.33$ [12] and -0.30 [13]). Δ^*_{cr} is plotted in the insert of Fig. 6 versus α (equation 7). A polynomial fit is provided for Δ^*_{cr} in the legend of Fig. 6.

The activation energy and the pre-exponential factor were calculated by varying T_W and fixing the other parameters. The slope and offset of the log $[\zeta F(\zeta)/(A\Delta^*_{cr})]$ versus $1/T_W$ plot yielded $E = 243.4$ kJ/mol and $B = 4.36 \times 10^5$ $(\text{kmol/m}^3)^{1.33}\text{s}^{-1}$, respectively. The activation energy is considerably higher than the accepted $E \approx 200$ kJ/mol [12,13]. The catalytic wall is, however, a sink for radicals and inhibits ignition; the wall flux of OH is net-adsorptive well before homogeneous ignition (see Ref. [5] and the OH profiles of Fig. 4). The fluxes of H and O are also adsorptive (there is no O or H desorption in the surface mechanism [7]). The inhibition is illustrated in Fig. 6; fuel conversion and OH profiles (similar to those of Fig. 2) are presented under two

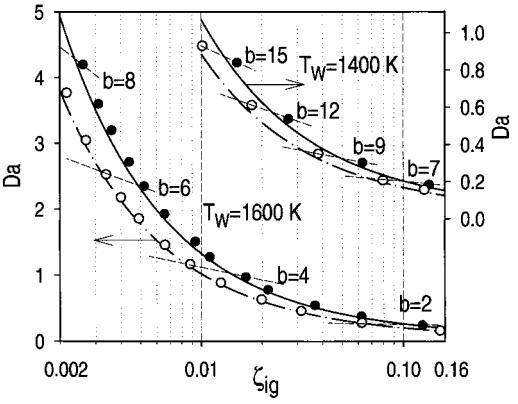

FIG. 7. Damköhler (Da) versus ignition distance (ζ_{ig}) plots for $T_{IN} = 623$ K and two wall temperatures. The $T_W = 1600$ K plot refers to the left Da axis and the $T_W = 1400$ K plot to the right axis. The lines are analytical predictions from equation 2. Solid lines, $\phi = 0.55$; dashed-dotted lines, $\phi = 0.35$. The symbols are full parabolic computations; solid circles, $\phi = 0.55$; open circles, $\phi = 0.35$. The halfwidth b ranges from 2 to 8 mm for the $T_W = 1600$ K, $\phi = 0.55$ case, and from 1.5 to 7 mm for the $T_W = 1600$ K, $\phi = 0.35$ case; the increment between successive b is 0.5 mm. The dashed lines join symbols with the same T_W and b.

conditions: normal surface reactions and surface reactions with the adsorption/desorption of OH and the adsorption of O and H removed. The removal of these reactions has no influence on the catalytic fuel conversion [5]. The x_{ig} is reduced by a factor of three in the latter case, explaining the higher apparent activation energy.

The proposed use of the ignition criterion is, under the parabolic limit $U_{IN} \geq U_{m,IN}$, as follows. Fig. 5 is first used to determine, for a desired percentage catalytic conversion, the required ζ (ζ is largely independent of b). Substituting ζ into equation 2, the Da and hence b are obtained. The calculated b provides the maximum halfwidth of a channel with a length ζ, for which homogeneous ignition is avoided. This information is of great interest in CSC as homogeneous ignition may cause meltdown. The agreement between analytical and numerical results over the entire range of parameter variation is very good. The b values calculated from equation 2 are within 9.2% of the computed values. This is also illustrated in the Da versus ζ_{ig} plots of Fig. 7; analytical (equation 2) and full parabolic computations are given. Equation 2 can be also applied to the reverse problem, that is, to determine ζ_{ig} given the b. Equation 2 is then implicit and is solved iteratively to provide ζ_{ig} (for $\zeta_{ig} \leq 0.16$). Criteria such as the above have not been reported in the literature; moreover, the accuracy is sufficient for engineering calculations.

Conclusions

The applicability of the boundary layer approximation in assessing homogeneous ignition in methane/air CSC was investigated with parabolic and elliptic numerical simulations. The parabolic approach is valid for inlet velocities U_{IN} greater than a minimum value $U_{m,IN}$ which depends mainly on the equivalence ratio ϕ; $U_{m,IN}$ have been calculated as a function of ϕ at atmospheric pressure. An analytical ignition criterion used in conjunction with a one-step gaseous reaction $B(C_{CH_4})^{n_F} \exp(-E/RT)$ predicts with accuracy better than 9.2% homogeneous ignition distances in methane CSC. The three parameters of the gaseous reaction are $n_F = -0.33$, $E = 243.4$ kJ/mol, and $B = 4.36 \times 10^5$ (kmol/m^3)$^{1.33}$s^{-1}.

Nomenclature

b	channel halfwidth
B	frequency factor of gaseous reaction (equation 1)
c_p	specific heat at constant pressure
Da	Damköhler number (diffusion over chemical time)
E	activation energy of gaseous reaction (equation 1)
Le	Lewis number of fuel (thermal over species diffusivity)
n_i, n	reaction order (i = F, O), total reaction order ($= n_F + n_O$)
Re	Reynolds number (equation 3)
q	heat of combustion per unit mass of fuel
W_i, $\bar{W}$	species molecular weight, average molecular weight
Y_i	species mass fraction

Greek symbols

α_{th}	thermal diffusivity ($\mu/\rho Pr$)
Δ_{cr}, Δ^*_{cr}	critical Damköhler number, critical ignition Damköhler number
ζ	non-dimensional streamwise distance (equation 3)
μ	viscosity
ν_i	species stoichiometric coefficient
ρ	density
φ	perturbation parameter for temperature (equation 6)
χ	transverse stretched coordinate (equation 6)
ω_F	fuel reaction rate (equation 1)

Subscripts

F, O, P	fuel, oxidizer, product
IN, ig	inlet, ignition

Acknowledgments

Financial support was provided by the Swiss Federal Office of Energy (BFE) under contract no. 59048 and Alstom Power and Technology of Switzerland.

REFERENCES

1. Dalla Betta, R. A., and Rostrup-Nielsen, T., *Catal. Today* 47:369–375 (1999).
2. Song, X., Williams, W. R., Schmidt, L. D., and Aris, R., *Combust. Flame* 84:292–311 (1991).
3. Ikeda, H., Libby, P. A., Williams, F. A., and Sato, J., *Combust. Flame* 93:138–148 (1993).
4. Bui, P. A., Vlachos, D. G., and Westmoreland, *Proc. Combust. Inst.* 26:1763–1770 (1996).
5. Dogwiler, U., Benz, P., and Mantzaras, J., *Combust. Flame* 116:243–258 (1999).
6. Dogwiler, U., Mantzaras, J., Benz, P., Kaeppeli, B., Bombach, R., and Arnold, A., *Proc. Combust. Inst.* 27:2275–2282 (1998).
7. Deutschmann, O., Schmidt, R., Behrendt, F., and Warnatz, J., *Proc. Combust. Inst.* 26:1747–1754 (1996).
8. Mantzaras, J., and Benz, P., *Combust. Flame* 119:455–472 (1999).
9. Brenan, K. E., Campbell, S. L., and Petzold, L. R., *Numerical Solution of Initial Value Problems in Differential-Algebraic Equations,* North-Holland, New York, 1989.
10. Raja, L. L., Kee, R. J., Deutschmann, O., Warnatz, J., and Schmidt, L. D., *Catal. Today* 59:47–60 (2000).
11. Warnatz, J., Maas, U., *Technische Verbrennung,* Springer-Verlag, Berlin, 1993, p. 102.
12. Lifshitz, A., Scheller, K., Burcat, A., and Skinner, G. B., *Combust. Flame* 16:311–321 (1971).
13. Westbrook, C. K., and Dryer, F. L., *Combust. Sci. Technol.* 27:31–43 (1981).
14. Griffin, T., Weisenstein, W., Scherer, V., and Fowles, M., *Combust. Flame* 101:81–90 (1995).
15. Bruno, C., Walsh, P. M., Santavicca, D. A., Sinha, N., Yaw, Y., and Bracco, F. V., *Combust. Sci. Technol.* 31:43–74 (1983).

COMMENTS

John W. Daily, University of Colorado at Boulder, USA. Please comment on the effect a non-uniform wall temperature would have on the validity of your analytical expressions as would occur under realistic operating conditions.

Author's Reply. Under realistic operating conditions, the front face of the channel exhibits lower surface temperatures (T_w) due to finite-rate surface kinetics and upstream surface radiation heat losses. These effects, along with heat conduction in the solid wall—the latter is of importance for lightoff—can be treated only with detailed computations such as those of our earlier work (Ref. [5] in paper). A further complication in methane CST arises from the implementation in practical devices of additional heat loss mechanisms (e.g., alternated active/inactive channels [Ref. 1 in paper]) necessary to avoid catalyst overheat driven by the nearly unity methane Lewis number.

The analytical criterion provides a conservative ignition distance compared to that of the ideal T_w-distribution, if the maximum of the ideal distribution is used as the criterion's constant wall temperature. However, the ideal T_w-distribution depends heavily on the particular system under investigation and its heat-loss mechanisms. Experimental input of an average T_w is desired, and this information is usually available even in realistic devices. Analytical ignition distances calculated with an the initial temperature ramp is short compared to the total channel length. This condition is satisfied in ignition catalysts with high equivalence ratio and/or high inlet temperature and especially in mid- or high-temperature catalysts. The latter have substantially higher inlet temperatures and nearly no upstream radiation heat losses resulting in a much more uniform wall temperature profile compared to that of an ignition catalyst. Finally, the criterion is currently extended to include finite-rate surface kinetic effects.

•

Johan Andrae, Royal Institute of Technology, Sweden. Have you considered effects of catalytic inhibition other than radical adsorption on the surface?

Author's Reply. Radical adsorption/desorption is the second in importance to gaseous ignition inhibition mechanism after the predominant near-wall fuel depletion inhibition. Other mechanisms that could contribute to the above inhibition are product formation (carbon monoxide or water) and radical recombination reactions on the wall. Discussion on these effects can be found, for example, in our earlier work (Ref. [5] in paper) and for the hydrogen system (Ref. [4] in paper), and in Markatou [1], to mention a few references.

It must be clarified, however, that the particular inhibition mechanisms are not relevant for the ignition criterion. The three gaseous reaction parameters presented in this work include all the inhibition (or promotion) mechanisms since they were determined by fitting analytical calculations to full gaseous and surface chemistry numerical predictions. In this respect, the precise nature of the inhibition mechanisms is irrelevant for the derivation of the analytical ignition criterion.

REFERENCE

1. Markatou, P., Pfefferle, L. D., and Smooke, M. D., *Combust. Flame* 93:185–201 (1993).

•

David K. Zerkle, Los Alamos National Laboratory, USA. You've stated that ignition parameters resulting from your simulations are independent of the Reynolds and Peclat numbers, yet the ignition location is highly dependent upon whether combustion radicals such as hydrogen atoms are quenched on the surface. This suggests that hydrogen-atom diffusion plays an important role in the ignition phenomenon. However, because $P_c = VL/D_{ae}$, your statements suggest that the ignition phenomenon is independent of D_{ae} (mass diffusion coefficient). Can you reconcile this apparent contradiction? Is there perhaps a length scale for ignition that is more appropriate than the channel diameter?

Author's Reply. We repeat the relevant sentence of our Results and Discussion section since the posed question totally misinterprets our statement: "It is emphasized that the controlling parameter in the above comparisons (*elliptic and parabolic predictions*) is the absolute magnitude of U_{IN} and not geometrical factors (b) or non-dimensional groups (such as *Re*) with an explicit geometric dependence." In summary, it was conclusively shown that the *Re* or Peclet (*Pe*) numbers play no role in the applicability of the parabolic approximation in assessing homogeneous ignition. The controlling parameter is, for a fixed equivalence ratio, U_{IN}.

The posed question misinterprets our statement by suggesting that the ignition parameters of our simulation (ignition location) are independent of *Re* and *Pe*. This is, of course, incorrect, as our ignition criterion of equation 2 has a very direct dependence on *Re* via ζ (see equation 3, ζ is inversely proportional to *Re*). In addition, the fuel mass diffusion coefficient enters the criterion via the Lewis number (*Le* (see equation 5). Hence, there is no contradiction of any kind in our initial statement. An additional *Le* or *Pe* number based on radical mass-transport coefficients (apart from the already-employed fuel *Le*) would require the mathematical formulation to include at least two more reactions: one gaseous reaction to account for radical (H or better OH) production or depletion and one surface reaction to account for net radical adsorption. This is certainly not possible within the context of matched activation energy asymptotics in non-homogeneous flows and, moreover, not necessary because the radical inhibition has been successfully accounted for in the determination of the gaseous reaction parameters (higher apparent activation energy). As to the final comment whether "there is a length scale for ignition more appropriate that the channel diameter," the relevant non-dimensional parameter of our analysis, $\zeta = x/(bRePr)$, includes not only the channel hydraulic diameter (b) but also the physical length scale, x.